AIP | Journal of Applied Physics

Presence of excited electronic state in CaWO4 crystals provoked by a tetrahedral distortion: An experimental and theoretical investigation

Lourdes Gracia, Valéria M. Longo, Laécio S. Cavalcante, Armando Beltrán, Waldir Avansi et al.

Citation: J. Appl. Phys. **110**, 043501 (2011); doi: 10.1063/1.3615948
View online: http://dx.doi.org/10.1063/1.3615948
View Table of Contents: http://jap.aip.org/resource/1/JAPIAU/v110/i4
Published by the AIP Publishing LLC.

Presence of excited electronic state in $CaWO_4$ crystals provoked by a tetrahedral distortion: An experimental and theoretical investigation

Lourdes Gracia,[1] Valéria M. Longo,[2,a)] Laécio S. Cavalcante,[2] Armando Beltrán,[1] Waldir Avansi,[3] Máximo S. Li,[3] Valmor R. Mastelaro,[3] José A. Varela,[2] Elson Longo,[2] and Juan Andrés[1,b)]

[1]*MALTA Consolider Team, Departament de Química Física i Analítica, Universitat Jaume I, Campus de Riu Sec, Castelló E-12080, Spain*

[2]*LIEC, Instituto de Química, Universidade Estadual Paulista, Laboratório Interdisciplinar de Eletroquímica e Cerâmica, P.O. Box 355, 14800-900, Araraquara, SP, Brazil*

[3]*Instituto de Física de São Carlos, USP, 13560-970, São Carlos, SP, Brazil*

(Received 20 April 2011; accepted 22 June 2011; published online 16 August 2011)

By combining experimental techniques such as x-ray diffraction, Fourier transform Raman, ultraviolet-visible, x-ray absorption near edge structure, extended x-ray absorption fine structure spectroscopy, and theoretical models, a general approach to understand the relationship among photoluminescence (PL) emissions and excited electronic states in $CaWO_4$ crystals is presented. First-principles calculations of model systems point out that the presence of stable electronic excited states (singlet) allow us to propose one specific way in which PL behavior can be achieved. In light of this result, we reexamine prior experiments on PL emissions of $CaWO_4$. © *2011 American Institute of Physics*. [doi:10.1063/1.3615948]

I. INTRODUCTION

The alkaline-earth tungstates AWO_4 ($A = Ca^{2+}$, Sr^{2+}, Ba^{2+}) belong to an important family of inorganic functional materials,[1] being the focus of great interest because its advantages, such as: unlimited resources, low cost and environmental friendliness. They continue attracting considerable attention because they are found to be fascinating systems possessing various technological applications, mainly including: microwave, scintillation, optical modulation, magnetic and writing-reading-creasing devices, humidity sensors, optical fibers, photoluminescence materials,[2,3] and promising nonlinear media for the transformation of the radiation wavelength in lasers,[4,5] or often, a combination of them. In addition, they have been extensively investigated as a self-activating phosphor emitting blue or green light under ultraviolet or x-ray excitation,[6,7] and they are good laser host materials.[8–10]

It is well known that the physical and chemical properties of materials are strongly correlated with some structural factors, mainly, the structural order–disorder in the lattice. The materials can be described in terms of the packing of the constituent clusters of the atoms which can be considered the structural motifs. A specific feature of tungstates with a scheelite structure is the existence of the $[WO_4]$ and $[AO_8]$ clusters as isolated tetrahedra and snub bisdisphenoid polyhedra into crystal lattice,[11] respectively. This tetragonal structure can be also understood in terms of a network of $[WO_4]$ clusters, linked by strong bonds […W–O–W…] between the neighboring clusters, whose internal vibration spectra provide information on the structure and order-disorder effects in the crystal lattices.[12,13] Breaking symmetry process of these clusters, such as distortions, breathings and tilts, create a huge number of different structures and subsequently different materials properties, and this phenomenon can be related to local (short), intermediate and long-range structural order−disorder. Therefore, for AWO_4 scheelite, the material properties can be primarily associated to the cluster constituents, and the disparity or mismatch of both clusters can induce structural order-disorder effects, which will significantly influence the luminescence properties of the scheelites-type tungstates.[14–16] This structural pattern is a characteristic key for all the AWO_4 scheelites.

Pioneering studies by Blasse *et al.*[17,18] on various inorganic complexes were the first to recognize that the polyhedral groups consisting of both transition metal and oxygen ions are responsible for photoluminescence (PL) properties in titanates, niobates, and tungstates.[18,19] Then, these distortions are crucial in understanding the properties of materials and this map is capable to show properties on the basis of its constituent clusters. Distorted clusters yield a local lattice distortion that is propagated along the overall material, pushing the surrounding clusters away from their ideal positions. Thus, distorted clusters must move for these properties to occur, changing the electronic distribution along the network of these polar clusters and this electronic structure dictates both optical and electrical transport properties, and plays a major role in determining its reactivity and stability. Structural perfection of the aforementioned materials is a factor which can determine the capability of their application as optical materials, in particular, the PL behavior.

Among this calcium tungstate, $CaWO_4$, is an important optical material, which remains center of attraction for crystal growers, radiologists, material scientists and physicists due to its luminescence, thermoluminescence, and stimulated Raman scattering behavior,[20–22] and has potential application in the field of photonics and optoelectronics. $CaWO_4$ is one of the most widely used phosphors

a)Electronic mail: valerialongo@liec.ufscar.br.
b)Electronic mail: andres@qfa.uji.es.

in industrial radiology and medical diagnosis,[23] and it can be employed for a variety of applications, e.g., tunable fluorescence and sensor for dark matter search.[24,25] In addition, the optical properties of metal tungstates with different morphologies have been studied.[26,27] Su *et al.*[28] have reported that the physical properties of $CaWO_4$ nanocrystals are size-dependent. Since single crystals tungstates are mainly synthesized at high temperatures from melt, they can contain defects due to thermally activated processes. The presence of such defects can influence their optical characteristics. Various methods have been employed to prepare calcium tungstate ($CaWO_4$), such as: traditional solid state reaction,[29] solvothermal method,[30,31] low temperature solution method,[3] spray pyrolysis route,[32] sol–gel method,[33–39] molten salt method,[40] the so-called polymeric precursor method,[41,42] electrochemical method,[43] microwave irradiation,[44] pulsed laser deposition,[45] and vapor-deposition method.[46]

We have obtained $CaWO_4$ crystals by means of microwave assisted hydrothermal method, allowing to faster reaction rates and shorter reaction times, thereby leading to an overall reduction in energy consumption.[47,48] These attributes, along with higher product yields and improved chemical selectivity, make microwave assisted techniques inherently green compared to conventional heating techniques. The use of microwave energy to heat and drive chemical reactions is growing at a rapid rate, with new and innovative applications in material sciences,[49–51] and nanotechnology.[52,53]

Irradiation of a semiconductor with light of energy equal to or larger than the bandgap energy leads to the generation of electron–hole pairs, which can subsequently induce redox reactions on the semiconductor. An ideal PL material should possess an adequate mobility for photostimulated electron–hole separation and transportation in crystal lattices, and suitable energy levels of band potentials. It is thought that this performance or the electron–hole separation ability of a semiconductor is closely related to the crystal structure. It is well known that the intrinsic emission of the $CaWO_4$ phosphor is a broad emission band centered at 520 nm, which is due to electronic transitions of the charge-transfer type between oxygen and tungstate within the anion complex $[WO_4]^{2-}$.[54] Moreover, some new optical properties of this classic phosphor can be obtained by doping with transition metal ions[55]or rare-earth ions.[56] Based on the molecular orbital theory, the excitation and emission bands of $CaWO_4$ can be ascribed to the transition from the $^1A_1$ ground-state to the high vibration level of $^1T_2$ and from the low vibration level of $^1T_2$ to the $^1A_1$ ground-state within the $[WO_4]^{2-}$ complex.[57] Previous studies have shown that the PL properties of phosphor are sensitive to synthetic conditions, morphologies, size, surface defect states, and so forth.[58,59] Changes of microstructure and size would modify the electronic structures of phosphor, promoting the formation of excited carriers from the valence band to the conduction band, which then relax their energy on the product surfaces, leading to variations in luminescence.

Density functional theory (DFT) and its extensions[60–62] have been shown to model the ground-state for a wide variety of compounds accurately. In particular, phase stability has been shown to be efficiently and accurately accessible through DFT computations in much different chemistry.[63–68] Our group have been involved in a research project devoted to understand the mechanism behind the PL emissions in scheelite based materials,[41,69,70] and a fundamental issue that remains far from being fully understood concerns the role of the electronic excited states or how the electronic excited states are involved in the PL behavior. In a recent paper we have revisited theoretically the excited electronic states in $SrTiO_3$,[71] and to the best of our knowledge, this approach has never been attempted before. These results suggested that it is important to investigate the roles of the excited electronic states in expressing their photofunctions.

Motivated by these conflicting experimental and theoretical results and with the aim to understand the PL process during the excitation process, in this work, we would like to provide a combination of both experimental and theoretical studies on the PL emission of the undoped $CaWO_4$. The question of the key role of the electronic state-dependent on the PL mechanism of these systems is discussed here. Quantum chemical methods are becoming more and more important in this context, as they can play an essential role in the analysis of optical properties. From an experimental side, x-ray diffraction (XRD), Fourier transform Raman (FT-Raman), ultraviolet-visible (UV-vis), x-ray absorption near edge structure (XANES), extended x-ray absorption fine structure (EXAFS), and PL spectroscopy has been carried out, while the electronic structures, band structure and bonding properties for both ground and excited states have been calculated and characterized. Fundamentally, it is important to explain the PL phenomenon by the presence of excited electronic states and how they can be associated to in-gap defect states, which give rise to the PL emissions. Our investigations may be helpful to comprehend both the structural favorable conditions before the photon arrival and the search for the PL mechanism during the excitation process in scheelite based materials.

II. COMPUTATIONAL METHODS AND MODELS

Calculations were performed with the CRYSTAL06 program package.[72] For the Ca and W atoms were used the 86-511d21 G and a pseudopotential basis sets, respectively, provided by the CRYSTAL basis sets library, and oxygen atoms have been described by the standard 6-31 G*, with the optimized exponent of the *d* shell $\alpha = 0.8$.

The Becke's three-parameter hybrid nonlocal exchange functional[73] combined with the Lee−Yang−Parr gradient-corrected correlation functional, B3LYP,[74] has been used. Hybrid density-functional methods have been extensively used for molecules, providing an accurate description of crystalline structures, bond lengths, binding energies, and band-gap values.[75] The diagonalization of the Fock matrix was performed at adequate *k*-points grids (Pack-Monkhorst 1976) in the reciprocal space. The thresholds controlling the accuracy of the calculation of Coulomb and exchange integrals were set to 10^{-8} (ITOL1 to ITOL4) and 10^{-14} (ITOL5), whereas the percent of Fock/Kohn-Sham matrices

mixing was set to 30 (IPMIX = 30).[72] The dynamical matrix was computed by numerical evaluation of the first-derivative of the analytical atomic gradients. The point group symmetry of the system was fully exploited to reduce the number of points to be considered. On each numerical step, the residual symmetry was preserved during the self-consistent field method (SCF) and the gradients calculation.

We use periodic models to find the ground and excited singlet electronic states to determine their electronic structure and the specific atomic states which makeup their corresponding energies. This information is used to understand the transitions associated with PL emission behavior. Any attempt to find excited states with triplet mutiltiplicity was unsuccessfully. Vibrational analysis has been made to ensure that there are no imaginary frequencies and the structure corresponds to a minimum for the ground and excited singlet states. The band structures have been obtained along the appropriate high-symmetry paths of the Brillouin zone for the tetragonal system.

The crystal type-scheelite has a tetragonal structure with space group ($I4_1/a$). The calcium ions are eightfold coordinated with the oxygen's atoms surrounding tungstate groups. The tungsten atoms are tetrahedrally coordinated with the oxygen's atoms, where the tetrahedral angles are slightly distorted (see Fig. 1).[76]

III. EXPERIMENTAL DETAILS

In this work, $CaWO_4$ powders were obtained by coprecipitation and processed using a microwave-hydrothermal method in the presence of polyethylene glycol (PEG). This method makes use of either modified domestic microwave units, which are inexpensive, relatively simple to operate, cost effective, and readily available. The typical synthesis procedure is described as follows: 5×10^{-3} mol of tungstic acid (H_2WO_4) (99% purity, Aldrich), 5×10^{-3} mol of calcium acetate monohydrate [$Ca(CH_3CO_2)_2.H_2O$] (99.5% purity, Aldrich) and 0.1 g of PEG (*Mw* 200) (99.9% purity, Aldrich) were dissolved in 100 mL of deionized water. Then 5 mL of ammonium hydroxide (NH_4OH) (30% in NH_3, Synth) was added in the solution until the *p*H value reached to 10. The aqueous solution was then placed in an ultrasound for 30 min at room temperature. In the sequence, the mixture was transferred into a Teflon autoclave which was sealed and placed into a microwave hydrothermal system (2.45 GHz, maximum power of 800 W). Microwave-hydrothermal conditions were kept at 140 °C for 30, 60, 120, 240, and 480 min using a heating rate fixed at 25 °C/min. The pressure into the autoclave was stabilized at 294 kPa. After the microwave-hydrothermal treatment, the autoclave was cooled to room temperature. The resulting solution was washed with de-ionized water several times to neutralize the pH of the solution (~7), and the white precipitates were finally collected. Using the same experimental conditions, the powders obtained were dried in a conventional furnace at 65 °C for 12 h.

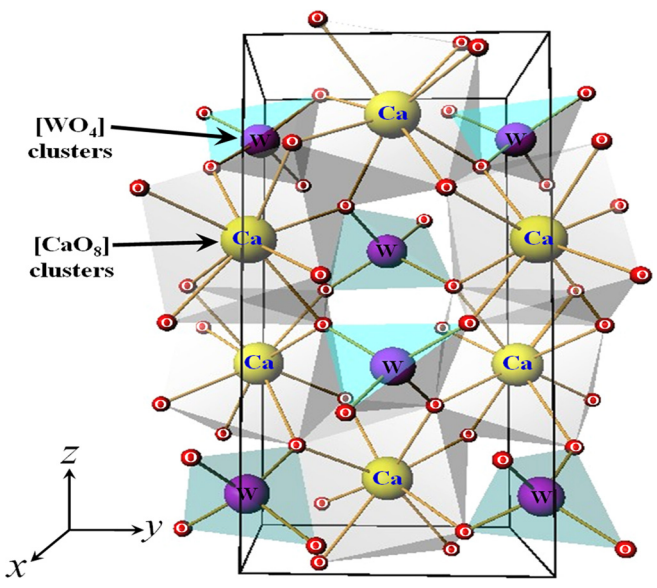

FIG. 1. (Color online) Representation of tetragonal structure for the $CaWO_4$ crystals formed by tetrahedral [WO_4] and deltahedral [CaO_8] clusters.

The $CaWO_4$ crystals were structurally characterized by x-ray powder diffraction (XRD) using a Rigaku-DMax/2500PC (Japan) with Cu-Kα radiation ($\lambda = 1.5406$ Å) in the 2θ range from 10° to 75 ° with scanning rate of 0.02°/s exposure total time of 15 min in normal routine. FT-Raman spectroscopy was recorded with a Bruker-RFS 100 (Germany). The spectra were obtained using a 1064 nm line of a Nd:YAG laser, keeping its maximum output power at 100 mW and performed in the range from 50 to 1000 cm^{-1}. UV-vis spectra were taken using a spectrophotometer of Varian, model Cary 5 G (USA) in diffuse reflection mode. PL measurements were performed through a Monospec 27 monochromator of Thermal Jarrel Ash (USA) coupled to a R446 photomultiplier of Hamamatsu Photonics (Japan). A krypton ion laser of Coherent Innova 90 K (USA) ($\lambda = 350$ nm) was used as an excitation source, keeping its maximum output power at 500 mW and maximum power on the sample after passing through from optical chopper of 40 mW. The electronic and local atomic structure around W atoms was checked by using the x-ray absorption spectroscopy (XAS) technique. The tungsten $L_{1,3}$ -edge x-ray absorption spectra of $CaWO_4$ crystals were collected at the LNLS (National Synchrotron Light Laboratory) facility using the D04B-XAFS1 beam line. XANES data were collected at the W $L_{1,3}$ in a transmission mode at room temperature using a Si(111) channel-cut monochromator. For XAS spectra measurements the samples were deposited on polymeric membranes and collected with the sample placed at 90° in relation to the x-ray beam. XANES spectrum was recorded for each sample using energy steps of 1.0 eV before and after the edge and 0.7 and 0.9 eV near of the edge region for W-L1 and L3 edge, respectively. The EXAFS spectra were measured from 100 eV below and 800 eV above the edge, with an energy step of 2 eV in preedge region, 0.5 in the near edge region and 1.0 eV in post-edge region with 2 s of integration time. Three EXAFS spectra of the samples were collected with the sample. All measurements were performed at room temperature. The analyses and theoretical calculations of XAS spectra were performed using IFEFFIT package.[77,78]

IV. RESULTS AND DISCUSSION

A. X-ray diffraction analyses

The polycrystalline nature of $CaWO_4$ crystals is expressed by XRD patterns as shown in Fig. 2, which were identified as a tetragonal structure in agreement with the respective inorganic crystal structure database (ICSD) No. 18135 (supporting information available).

The facility and low temperature synthesis of $CaWO_4$ related to the fast reaction due to the microwave coupling which allow a uniform solution heating start-up.[79,80] Compared with the usual methods, microwave-assisted synthesis has the advantages of shortening the reaction time and producing products with a small particle size, narrow particle size distribution and high purity.

B. XANES and EXAFS spectra analyses

The analyses of the XANES spectra has been used in order to obtain short- and medium range structural information in a large variety of materials such as simple and complex polycrystalline or amorphous oxide perovskites and glassy samples.[81–83] As presented before, the observation of the PL phenomenon in the AWO_4 compounds is mainly dependent on the structural organization at different levels, short, medium and at long-range order. Longo *et al.*[84,85] have used the XANES technique to characterize the local disorder in materials presenting an order−disorder phenomena. Figures 2(a) and 2(b) show the WL_1-edge and WL_3-edge XANES spectra, respectively, of $CaWO_4$ samples as a function of the annealing temperature and the WO_3 monoclinic phase, used as reference compound.

The W L_1-edge XANES spectrum provides information on the electronic state and the geometry of the tungsten species.[86–89] The intensity of pre-edge peak, indicated in Fig. 2(a) as X, is very sensitive to symmetry of the W atoms.[87–90] According to the literature,[87–90] the preedge peak is due to electronic transitions from 2*s* to 5*d* (W) orbital, which is dipole forbidden in the case of regular octahedra but allowed for distorted octahedra and tetrahedral. The WO_3 (reference compound) exhibit small preedge peaks due to distorted octahedral [WO_6] clusters [inset in Fig. 3(a)], in good agreement with previous reports.[87–89] In contrast, the as-synthesized samples ($CaWO_4$) exhibit a more intense pre-edge peak relate to tetrahedral [WO_4] clusters [inset in Fig. 3(a)], indicating that tungsten atoms are coordinated by four oxygen atoms.[86–89] The higher intensity of the preedge peak of $CaWO_4$ crystals indicates a higher symmetry of W sites when compared to WO_3 compound. As can also be observed on Fig. 3(a), no significant change is noted on the XANES spectra of $CaWO_4$ crystals as the treatment time of synthesis increases.

As it can observed in Fig. 3(b) the XANES spectra in the W-L_3 edge, the as-synthesized samples presents a different XANES spectrum compared to reference compound (WO_3). For the W-L_3 edge the white line mostly derives from electron transitions from the 2*p* 3/2 state to a vacant 5*d* state, as indicated in Fig. 3(b) as Y. According to the Yamazoe *et al.*[89] the form and the shape of white line depend on the particular structure of this compound. So, this difference is expected because as observed in Fig. 3(b), the WO_3 compound

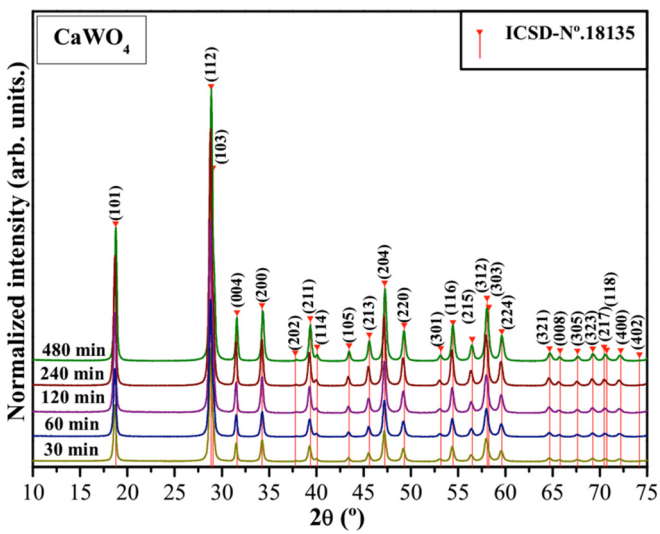

FIG. 2. (Color online) XRD patterns of $CaWO_4$ crystals processed at 140 °C for in the range of 30 to 480 min.

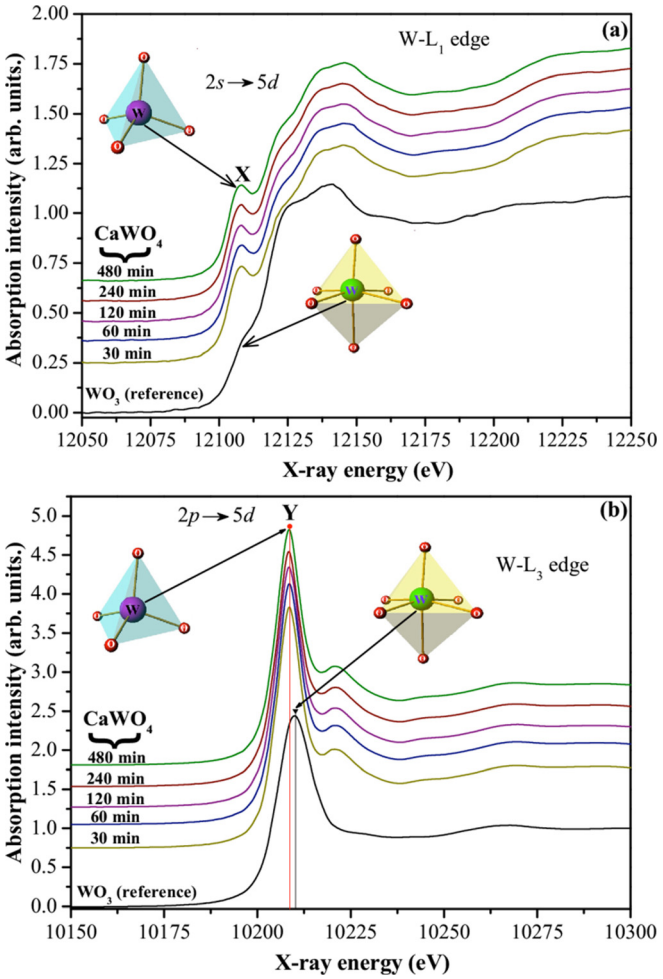

FIG. 3. (Color online) XANES spectra in the (a) W-L_1 edge; and (b) W-L_3 edges for $CaWO_4$ samples obtained by CP method and processed in MH system at 140 °C for different times (from 6 to 480 min) and the WO_3 monoclinic structure (Sigma-Aldrich-99.9% purity) used as standard compound.

has a W atom in an octahedral environment [Inset in Fig. 3(a)]. Moreover, we can observe a maximum value in the preedge peak (▼) at approximately 10 210 eV, while de $CaWO_4$ crystals present a tetrahedral environment [Inset in Fig. 3(a)], with a maximum value in the preedge Y peak (●) at approximately 10 208 eV. As shown previously in W-L_1 edge [Fig. 3(a)], we have observed no significant change of XANES spectra in the W-L_3 edge for the $CaWO_4$ crystals processed at 140 °C for different times in MH system [Fig. 3(b)].

According to the qualitative analyses of the $L_{1,3}$- XANES spectra of $CaWO_4$ crystals, it can assert that the first coordination shell around tungsten atoms is formed by four oxygen atoms in a quite regular structure independently of the synthesis conditions.[86–89,91,92] The similarity of the post-edge XANES spectra in the as-synthesized compounds also indicates that second and further coordination shells are quite similar.

The local order of the as-synthesized samples also was studied in EXAFS region of XAS spectra. Experimental W L_3-edge EXAFS signals $\chi(k)K^1$ and their Fourier transforms (FT) of the $CaWO_4$ crystals and reference compound are shown in Figs. 4(a) and 4(b), respectively.

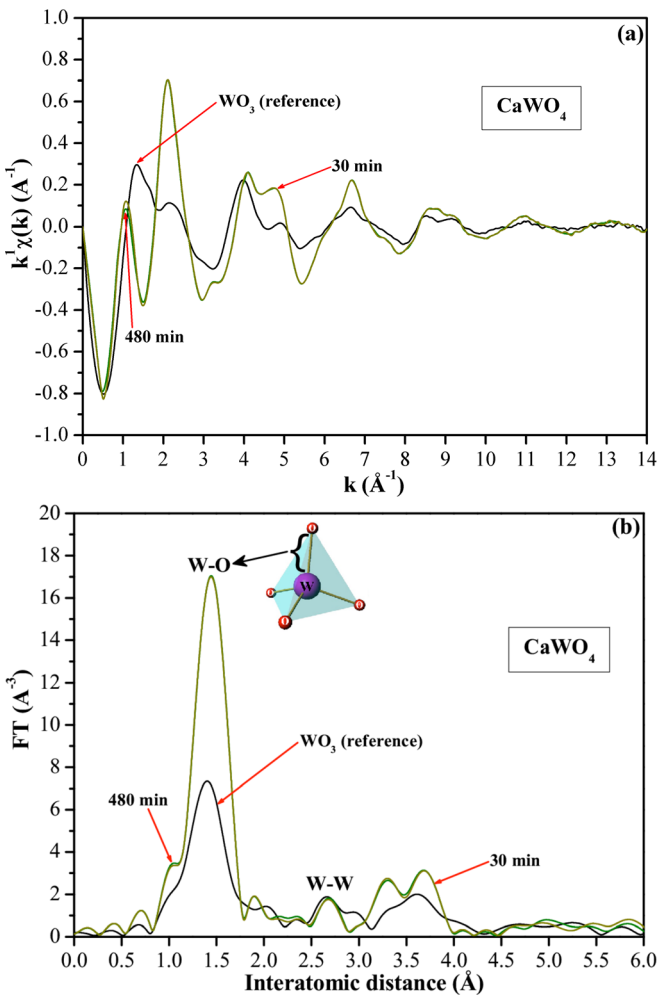

FIG. 4. (Color online) (a) Experimental W-L edge EXAFS signals $\chi(k)k^1$ for the reference compound (WO_3), the as-obtained samples; and (b) experimental uncorrected with Fourier transformed (FT) curve of reference compound (WO_3) and the as-obtained samples. The curves are obtained in the 3.5-14 $Å^{-1}$ *k*-space using a hanning window.

TABLE I. Structural results obtained from the fitting of the inverse of the FT concerning the first W–O coordination shell.

Sample	CN	R(Å)	σ^2(Å)	S_0^2	R-factor
30 min	4	1.787 ± 0.003	0.001 ± 0.001	0.084 ± 0.07	0.0047
480 min	4	1.787 ± 0.006	0.001 ± 0.001	0.85 ± 0.08	0.0049

As expected, the EXAFS spectra [Fig. 4(a)] of the as-prepared samples differ significantly of reference compound. Variations in the local structure of W are clearly depicted in the FT shown in Fig. 4(b), which display the radial structure functions for the central absorbing W atom. It is to be noted that the structure below 1 Å may arise from atomic XAFS and/or multielectron excitations, and it does not usually correspond to real coordination spheres. The peak around 1.4 Å, uncorrected from phase shift, corresponds to the first W coordination shell where anions of oxygen atoms surrounding the central atom.[86,87] The group of peaks at 3 Å are mainly due to the second and third shell, composed of tungsten and A 2 + atoms.[86,87] Synthesized $CaWO_4$ crystals present a higher FT intensity when compared with reference compounds, WO_3. In WO_3 compound the W atoms are located in a distorted octahedral [WO_6] clusters environment with W–O distances ranging from 1.77 to 2.20 Å, whereas in $CaWO_4$ crystals polycrystalline compound, tungsten atoms are located in a WO_4 regular tetrahedral unit (4 W–O distances at 1.70 Å).[93] Table I present the best fitting results of EXAFS spectra of both samples. The structural parameters used to start the fitting procedure of the EXAFS spectra obtained from ICSD No. 18135 file was based in structure where W atom are located in a WO_4 regular tetrahedral unit with 4 W–O bond-lengths around 1.771 Å. The fitting procedure for both samples was computed considering the following parameters: distance (ΔR), Debye-Waller factor (σ^2) and amplitude reduction factor (S_0^2). The other parameter, E_0, were obtained from the fitting of the sample obtained with 480 min, where E_0 has been found to be displaced a few electronvolts (8.1 ± 1.3) with respect to the edge inflection point, and was fixed for an analysis of sample obtained with 30 min. According to the fitting results presented in Table I, the average W–O distances for the both samples changed of obtained from ICSD No. 18135. The good quality of the theoretical fitting can be observed by the low value of R-factor, observed in Table I. In good agreement with XANES spectra, from Fig. 4(b), it is clear the strong octahedral distortion on the [WO_6] clusters of the WO_3 standard compound, while in $CaWO_4$ crystals a more regular symmetry was observed. For the as-obtained $CaWO_4$ crystals with the increase of MH processing time from 30 to 480 min, no significant change is noted in EXAFS spectra and experimental uncorrected FT curve, confirming that local order of as-obtained samples is similar, independently of synthesis conditions.

C. Analysis of the theoretical results

Table II shows the theoretical optimized distances Ca–O and W–O in Å and O–W–O angles in degrees for the ground singlet (s) and excited singlet (s*) electronic states.

TABLE II. Optimized lattice parameters, bond distances (multiplicity in parenthesis) and angles between bonds for the ground singlet (s) and excited singlet (s*) electronic states.

$CaWO_4$ clusters	Singlet (s)	Excited singlet (s*)
($a=b$) (Å)	5.202	5.244
(c) (Å)	11.291	11.121
(Ca–O) (Å)	2.433(4)	2.418(4)
(Ca–O) (Å)	2.466(4)	2.444(4)
(W–O) (Å)	1.751(4)	1.788(4)
α (O–W–O) (°)	114.01	117.23
β (O–W–O) (°)	107.25	105.74

The calculated distance values between W–O of 1.751 Å are in very good agreement with the EXAFS experimental result of 1.70 Å. The scheelite structure in s* state expanded somewhat in the a and b directions to $a=5.244$ Å, while contracting in the c direction to $c=11.121$ Å. The distortion of WO_4 entities becomes more noticeable in s* state with more difference in angles O–W–O (11.5° vs 6.7° in s fundamental structure). Total energy variation between s* and s states is 0.31 eV.

D. FT-Raman spectroscopy analyses

The degree of structural order at short-range can be available by Raman spectroscopy given information of small distortion. This technique is one of the most suitable methods for investigating and characterizing semiconductor structures. This spectroscopy is a sensitive indicator of structure and symmetry in solids and has proved to be useful in the study of phase transitions as a function of temperature, pressure[94,95] and composition.[96,97]

Figure 5 shows the FT-Raman spectra for the $CaWO_4$ crystals processed at 140 °C for different times from 30 to 480 min.

The scheelite crystal has symmetry (C_{4h}^6) at room temperature. The internal vibration is associated to the movements inside the WO_4 molecular group. The external or lattice phonons correspond to the motion of the Ca cation and the rigid molecular unit (translational modes).[4] Vibrational modes characteristic of the scheelite phase in the tetrahedral structure were observed for all samples. According to a group theory analysis, there are four vibration modes for ideal T_d symmetry: $\Gamma=A_1(\nu_1)+E(\nu_2)+F_2(\nu_3)+F_2(\nu_4)$. $A_1(\nu_1)$ vibration is the symmetric stretching mode, $F_2(\nu_3)$ is the antisymmetric stretching mode, and the $E(\nu_2)$ and $F_2(\nu_4)$ vibrations are bending modes. Since the factor groups of $CaWO_4$ are of lower symmetry than T_d, and the tetrahedral point groups themselves are nonideal, the doubly degenerate $E(\nu_2)$ and triply degenerate $F_2(\nu_4)$ vibrations split into the nondegenerate bands and give 26 vibrations, $\Gamma=3A_g+5A_u+5B_g+3B_u+5E_g+5E_u$. The samples present several peaks referring to the Raman-active internal modes of $[WO_4]$ tetrahedra: $\upsilon_1(A_g)$, $\upsilon_3(B_g)$, $\upsilon_3(E_g)$, $\upsilon_4(E_g)$, $\upsilon_4(B_g)$, $\upsilon_2(B_g)$, $\upsilon_2(A_g)$, $R(A_g)$, $R(E_g)$, and external T-(B_g, E_g, E_g) modes that are in agreement with the results reported by Campos *et al.*[69] and Hazen *et al.*[98] Table III reports normal vibrational modes active in Raman for s and s* states and experimental results. The small shifts observed on the positions of Raman modes can arise from different factors, such as: preparation methods, average crystal size, interaction forces between the ions or the degree of structural order in the lattice.[99] Moreover, the well-defined active-Raman modes confirm that $CaWO_4$ crystals are structurally ordered at short-range and independent of the processing time employed in the hydrothermal microwave treatment.

In crystals with the scheelite structure, the indicator of distortion of surroundings of the tetrahedral anion is the highest-frequency A_g vibration, which is a result of the Davydov splitting of the $(A_1)\nu_1$ free tetrahedral anion.[100,101] The A_g mode in fundamental s state is 312 cm^{-1}. This value is consistent with those reported previously of 335 cm^{-1} by experiments of pulsed laser ablation[102] and 276 cm^{-1} microwave hydrothermal treatments. In passing from s to s* state the A_g mode increases to 324 cm^{-1} as well as enlarges the length of the W–O bond.

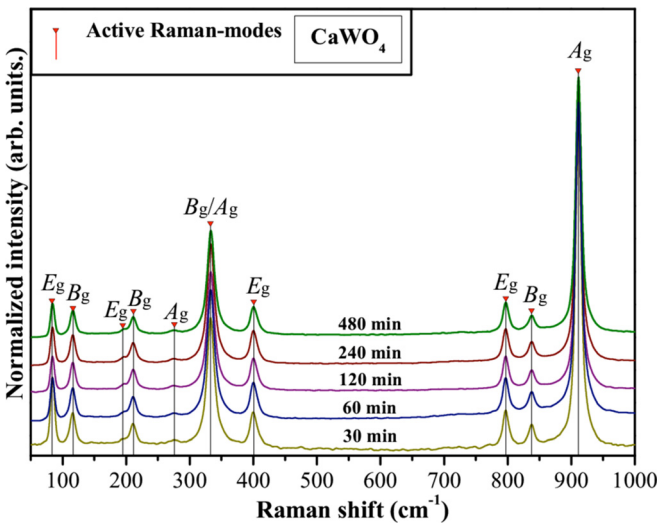

FIG. 5. (Color online) FT-Raman spectra in the range from 50 to 1000 cm^{-1} of $CaWO_4$ crystals processed at 140 °C for different times in MH system.

TABLE III. Vibrational Raman modes in (cm^{-1}) for experimental and theoretical ground singlet (s) and excited singlet (s*) electronic states.

Attribution and Symmetry	$CaWO_4$ (Ref. 85)	$CaWO_4$	Theoretical (s)	Theoretical (s*)
[$\nu_1(WO_4)$-A_g]	912	911	936	873
[$\nu_2(WO_4)$-B_g]	838	838	792	730
[$\nu_2(WO_4)$-E_g]	797	797	737	678
[$\nu_3(WO_4)$-B_g]	409	___	505	512
[$\nu_3(WO_4)$-E_g]	401	401	494	482
[$\nu_4(WO_4)$-A_g]	336	333	442	434
[$\nu_4(WO_4)$-B_g]	336	333	408	404
E_g	___	___	343	380
R[(WO_4)]-A_g	275	276	312	324
R[(WO_4)]-E_g	218	___	220	219
B_g	210	212	216	212
E_g	195	195	148	150
B_g	117	116	118	123
E_g	84	84	___	___

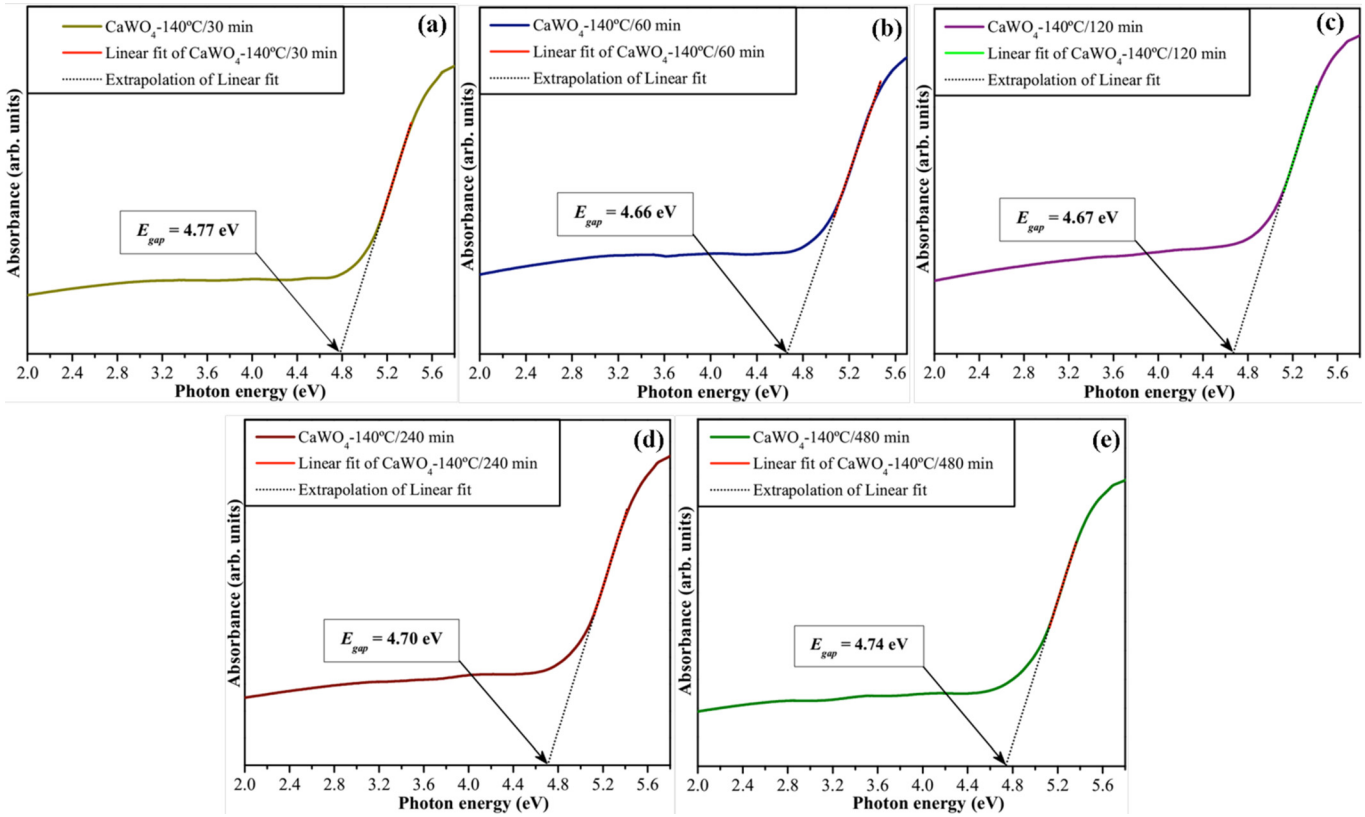

FIG. 6. (Color online) UV-vis spectra dependent of the absorbance for the $CaWO_4$ crystals processed at 140 °C for different times in MH system.

E. UV-vis measurements analysis

The absorbance spectral dependence of $CaWO_4$ crystals processed at 140 °C from 30 to 48 min in MH system is illustrated in the Figs. 6(a)–6(e). The optical bandgap is related to the absorbance and the photon energy by the following Eq. (1):

$$h\nu\alpha \propto (h\nu - E_{\text{gap}})^{1/2}, \tag{1}$$

where α is the absorbance, h is the Planck constant, ν is the frequency and E_{gap} is the optical bandgap.[103] The bandgap values of $CaWO_4$ crystals were evaluated by extrapolating the linear portion of the curve. The entire sample presents a well-defined interband transition with a quasivertical absorption front which is typical of semiconductor crystalline materials.

There is a significant difference between the values of bandgap obtained in this work and those reported before for our group (5.27 eV).[104] The exponential optical absorption edge and the optical bandgap energy are controlled by the degree of structural disorder in the lattice. The decrease in the bandgap can be attributed to defects, local bond distortion, intrinsic surfaces states and interfaces which yield localized electronic levels in the forbidden bandgap.[105,106] We believe that this significant difference is attributed to surface and interface intrinsic defects generally expected in the MH processing.[107,108]

F. PL emission analyses

Figure 7 illustrates the PL spectra recorded at room temperature for the $CaWO_4$ crystals processed at 140 °C for different time (from 30 to 480 min) in MH system. The insets show the digital photos for the PL emission of $CaWO_4$ crystals.

PL spectra present a broad band covering the visible electromagnetic spectra in the range from 350 to 800 nm, and the profile of the emission band is typical of a multiphonon and multilevel process; i.e., a system in which relaxation occurs by several paths involving the participation of numerous states within the bandgap of the material.

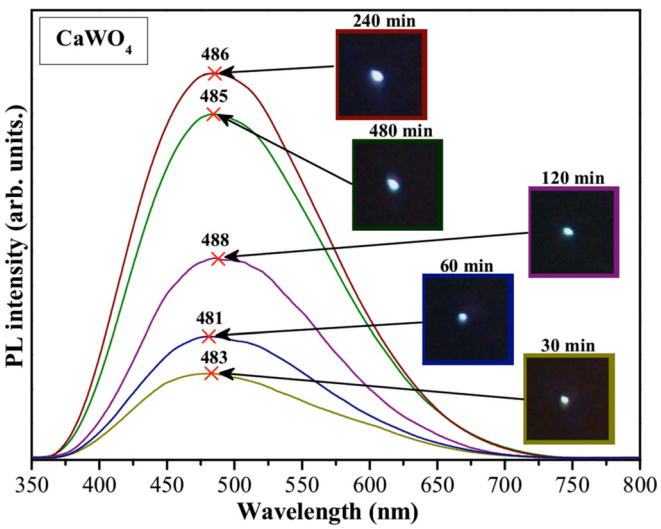

FIG. 7. (Color online) PL spectra of $CaWO_4$ crystals processed at 140 °C for different times (from 30 to 480 min) and excited by a krypton ion laser ($\lambda = 350$ nm).

Disorder in materials can be manifested in many ways; examples are vibrational, spin and orientation disorder (all referred to a periodic lattice) and topological disorder. Topological disorder is the type of disorder associated with glassy and amorphous solid structures in which the structure cannot be defined in terms of a periodic lattice. PL is a powerful probe of certain aspects of short-range order in the range 2–5 Å and medium range 5–20 Å such as clusters where the degree of local order is such that structurally inequitable sites can be distinguished due to its different types of electronic transitions and are linked to a specific structural arrangement.

The PL spectra of tungstates are often decomposed in blue, green and red contributions. However, there exist various controversial interpretations on tungstate PL spectra mainly about its green typical maximum contribution. Blasse and Wiegel[109] and Korzhik *et al.*[110] concluded that green emission originates from WO_3 center. Sokolenko *et al.*[111] attributed green-red emission to WO_3, $V_O^{\bullet\bullet}$ oxygen-deficient complexes. Sienelnikov *et al.*[112] suggest that distorted tetrahedral $[WO_4]$ clusters induced the formation of oxygen vacancies are responsible for the green luminescence band. Otherwise, it is generally assumed that the measured emission spectrum of $CaWO_4$ crystals is mainly attributed to the charge-transfer transitions within the $[WO_4]^{2-}$ complex in ordered systems[30,31,69,113–115] or complex cluster vacancies $[WO_3.V_O^z]$[116–118] and $[CaO_7.V_O^z]$[117] (where $V_O^z = V_O^x, V_O^{\bullet} or V_O^{\bullet\bullet}$).

In our work, it was found a wide PL emission with maximum picked in the blue area of visible spectra of light. This emission was quite different from previous results of crystalline $CaWO_4$ powders synthesized by the polymeric precursor method were the PL emission has a maximum centered at 520 nm, the green area of visible spectra.[69,104] Both $CaWO_4$ crystals, obtained by processing in MH system and polymeric precursor method, were crystalline at long range order in agreement with XRD analyses. However, the difference in the maximum PL emission between the samples obtained by the two methods show that there are structural differences between them. Disorders in surfaces and interfaces commonly occur in materials synthesized by the microwave-assisted hydrothermal method and created additional levels above the valence band and below the conduction band, decreasing the bandgap.[6,108,119,120] In this case, the decrease of the bandgap, as showed by the UV-vis measurements, leads to the dislocation of the natural scheelite green emission to blue emission.

G. Band structure and density of states (DOS)

In Fig. 8 are shown the band structures and DOS for s and s* structures, with direct band gaps of 5.71 eV and 5.21, respectively. A considerable decrease of the bandgap energy is observed (0.5 eV) with respect to the s fundamental state. The distortion process on the fundamental $[WO_4]_d$ and $[CaO_8]_d$ clusters to the excited $[WO_4]_d^*$ and $[CaO_8]_d^*$ tetrahedral and deltahedral groups, respectively, favors the formation of intermediary energy levels in the conduction band (CB) which confer the bandgap of this material. An analysis of the DOS projected on atoms and orbitals shows that the

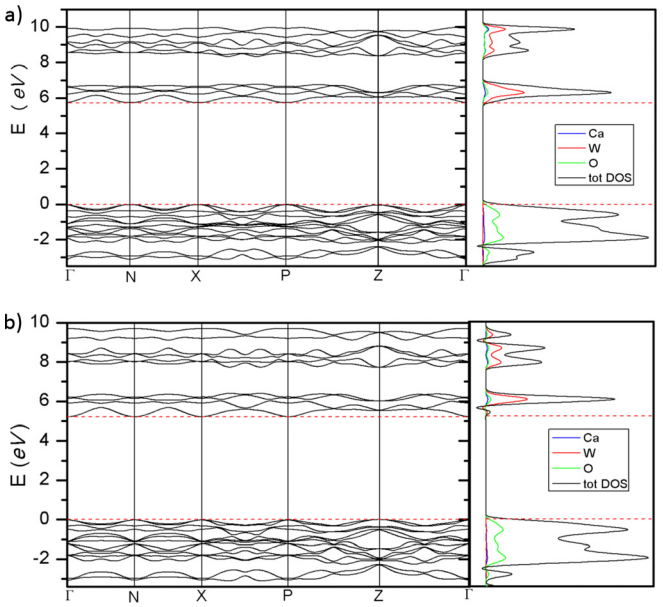

FIG. 8. (Color online) Band structures and DOS for the (a) singlet in fundamental state; and (b) singlet excited.

valence band (VB) maximum is derived mostly from O $2p$ ($2p_y$ and $2p_z$) orbitals for fundamental and excited states. The CB in the fundamental state is composed by $5\,d_{z^2}$ over $5\,d_{x^2-y^2}$ in a first set of CB and by $5\,d_{xy}$ in a second CB. As a difference of fundamental state, in the singlet excited state there is a first CB with dominance of W $5\,d_{x^2-y^2}$ over W $5\,d_{z^2}$ contribution. However, it appears new energy levels lower in energy previous this first CB precisely composed by theses $5\,d_{z^2}$ states that can be understood as intermediary levels. A second CB can be found which is governed by W $5\,d_{yz}$ orbitals.

Therefore, an analysis of site- and orbital-resolved DOS shows a significant dependence of the W CB DOS's on the local coordinations. During the excitation process some electrons are promoted more feasibly from the oxygen $2p$ states ($2p_y$ and $2p_z$) to these tungsten $5d$ states ($5\,d_{z^2}$) through the absorption of photons. The emission process of photons occurs when an electron localized in a tungsten $5d$ state decays into an empty oxygen $2p$ state. Then the PL emission can be attributed to this mechanism which is derived from distorted $[WO_4]_d$ and $[CaO_8]_d$ preexisting clusters.

H. Wideband model

The theoretical results point out that a symmetry breaking process, associated to order–disorder effects, is a necessary condition for the presence of PL emission. These structural changes can be related to the charge of polarization between distorted clusters that are capable to populate stable excited electronic states. Central to the observation of the PL phenomena in $CaWO_4$ crystals is the localization and characterization of excited states that can be considered as trap states implicated in this process. Once these excited states are populated, they may return to lower energy and ground states via radiative and/or nonradiative relaxations. Therefore, the PL process is understood in a first step as an

excitation from the fundamental state (singlet) to a higher energy state (excited singlet). The second step corresponds to an intersystem crossing process from the excited singlet to fundamental singlet electronic state. Once this singlet electronic is sufficiently populated, an intersystem crossing process involving the excited states can occur; finally, the PL emission takes place with concomitant return to a ground state.

Then we can identify two effects in the PL emission of the $CaWO_4$ crystals samples. The first effect is intrinsic to scheelite material and derived from the bulk material that is constituted by of asymmetric distorted $[WO_4]_d$ tetrahedra and $[CaO_8]_d$ deltahedra which allows to the excited $[WO_4]_d^*$ and $[CaO_8]_d^*$ tetrahedra and deltahedra groups, respectively. These excited states favor the population of intermediary energy levels within the bandgap of this material and are linked to the universal greenish scheelite luminescence. The second effect is a consequence of the surfaces and interfaces complex clusters defect that produce extrinsic defects that also decrease the bandgap and allows to the blue-emission. The interplay between these clusters and defects generates a specific PL emission color.

Based on the findings made, we propose an expanded model derived from the wide-band model,[85,121] to explain the PL behavior. Before the photon arrival, the short and intermediate range structural defects generate localized states within the bandgap and a nonhomogeneous charge distribution in the cell. After the photon arrival, the lattice configuration changes (like a "breath") and distorted excited clusters are formed allowing electrons to become trapped. In the final state the photon decay by radiative or nonradiative relaxations.

On a technical level, a clear area of improvement is the theoretical description of the excited electronic states. Rationalizing the chemical nature of excited electronic states is not an easy task and in the present work the excited states have been localized and characterized at DFT calculation level. This is a very strong restriction that can be assumed as a limiting case, the theoretical description of physical/chemical processes that take place in excited electronic states needs a method that can describe in a balanced way all of the electronic states involved, including both statistical and dynamical effects to quantitatively asses these states. This aim can be reached using a more sophisticated and computationally demanding calculation level, such as multi-configuration based methodology. However, the present model can be considered a shift toward a better understanding of PL phenomena in scheelite based materials in general. Although the small models described herein may not capture the full extent of the optical process, they do reveal some of the sorts of structural order–disorder effects before and after the photon arrival that could contribute significantly to PL emissions.

V. CONCLUSIONS

In summary, optical properties of the $CaWO_4$ crystals are studied by a different experimental techniques and first principle calculations. Clear evidence of a relationship between PL emissions and order–disorder effects is disclosed, and it is associated to structural distortions of both ideal $[WO_4]$ tetrahedra and $[CaO_8]$ deltahedra as a constituent clusters of $CaWO_4$.

Present work enlightens the central role of the excited electronic states during the PL emission. This interpretation is supported by the localization and characterization of a stable electronic excited state (singlet, s^*). We have characterized the normal vibrational modes associated to the tetrahedral distortions involved in the achievement of s^* excited state.

These results provide new insight into PL properties and have profound implications to design controlled structures with innovative optical applications. It is our intention to extend our studies to different scheelite based materials, including also different types of excitations, and the present result may provide a general strategy for a better understanding of PL phenomena in these materials. We hope that this study will stimulate experimental efforts toward the confirmation of the present findings.

ACKNOWLEDGMENTS

This work is supported by the Spanish MALTA-Consolider Ingenio 2010 Program (Project CSD2007-00045), Bancaixa Foundation (P11B2009-08), Spanish-Brazilian Program (PHB2009-0065-PC), Ciencia e Innovación for project CTQ2009-14541-C02, Generalitat Valenciana for Prometeo/2009/053 project, and by the financial support of the Brazilian research financing institutions: CAPES, CNPq, and FAPESP. This work was partially realized at the LNLS, Campinas, S.P. Brazil. The authors also acknowledge the Servei Informatica, Universitat Jaume I for generous allotment of computer time.

[1]Y. X. Zhou, H. B. Yao, Q. Zhang, J. Y. Gong, S. J. Liu, and S. H. Yu, Inorg. Chem. **48**(3), 1082 (2009).
[2]A. Phuruangrat, T. Thongtem, and S. Thongtem, Curr. Appl. Phys. **10**(1), 342 (2010).
[3]S. H. Yu, B. Liu, M. S. Mo, J. H. Huang, X. M. Liu, and Y. T. Qian, Adv. Funct. Mater. **13**(8), 639 (2003).
[4]T. T. Basiev, A. A. Sobol, Y. K. Voronko, and P. G. Zverev, Opt. Mater. **15**(3), 205 (2000).
[5]T. T. Basiev, P. G. Zverev, A. Y. Karasik, S. V. Vassiliev, A. A. Sobol, D. S. Chunaev, V. A. Konjushkin, A. I. Zagumennyi, Y. D. Zavartsev, S. A. Kutovoi, V. V. Osiko, and I. A. Shcherbakov, Trends Opt. Photonics **94**, 298 (2004).
[6]L. S. Cavalcante, J. C. Sczancoski, J. W. M. Espinosa, J. A. Varela, P. S. Pizani, and E. Longo, J. Alloys Compd. **474**(1–2), 195 (2009).
[7]T. Thongtem, A. Phuruangrat, and S. Thongtem, Appl. Surf. Sci. **254**(23), 7581 (2008).
[8]I. Hemmati, H. R. M. Hosseini, and A. Kianvash, J. Magn. Magn. Mater. **305**(1), 147 (2006).
[9]H. Shokrollahi and K. Janghorban, J. Mater. Process. Technol. 189(1–3), 1 (2007).
[10]T. Yamamoto, M. Niwano, and E. Nakagawa, U.S. Patent 5, 116, 437 (1992).
[11]R. W. G. Wyckoff, *Crystal Structures* (Wiley, New York, 1948), Vol. II, Chap. 8.
[12]A. Phuruangrat, T. Thongtem, and S. Thongtem, J. Cryst. Growth **311**(16), 4076 (2009).
[13]A. Phuruangrat, T. Thongtem, and S. Thongtem, J. Phys. Chem. Solids **70**(6), 955 (2009).
[14]S. Chernov, D. Millers, and L. Grigorjeva, Phys. Status Solidi C **2**(1), 85 (2005).

[15]M. Itoh and M. Fujita, Phys. Rev. B **62**(19), 12825 (2000).
[16]M. Nikl, P. Bohacek, E. Mihokova, M. Kobayashi, M. Ishii, Y. Usuki, V. Babin, A. Stolovich, S. Zazubovich, and M. Bacci, J. Lumin. **87**(9), 1136 (2000).
[17]J. A. Groenink and G. Blasse, J. Solid State Chem. **32**(1), 9 (1980).
[18]B. Bouma and G. Blasse, J. Phys. Chem. Solids **56**(2), 261 (1995).
[19]G. Blasse, Prog. Solid State Chem. **18**(2), 79 (1988).
[20]F. Lei, B. Yan, and H. H. Chen, J. Solid State Chem. **181**(10), 2845 (2008).
[21]M. Nikl, Phys. Status Solidi A **178**(2), 595 (2000).
[22]S. H. Yu, M. Antonietti, H. Colfen, and M. Giersig, Angew. Chem., Int. Ed. **41**(13), 2356 (2002).
[23]F. Forgaciu, E. J. Popovici, C. Ciocan, L. Ungur, and M. Vadan, Sioel'99: Sixth Symposium on Optoelectronics. Necsoiu, T Robu, M Dumitras, DC, Bucharest, Romania. 4068, 124-129 (2000).
[24]S. Cebrian, N. Coron, G. Dambier, P. de Marcillac, E. Garcia, I. G. Irastorza, J. Leblanc, A. Morales, J. Morales, A. O. de Solorzano, J. Puimedon, M. L. Sarsa, and J. A. Villar, Phys. Lett. B **563**(1–2), 48 (2003).
[25]M. V. Nazarov, D. Y. Jeon, J. H. Kang, E. Popovici, L. E. Muresan, M. V. Zamoryanskaya, and B. S. Tsukerblat, Solid State Commun. **131**(5), 307 (2004).
[26]B. Liu, S. H. Yu, L. J. Li, Q. Zhang, F. Zhang, and K. Jiang, Angew. Chem., Int. Ed. **43**(36), 4745 (2004).
[27]Q. Zhang, W. T. Yao, X. Y. Chen, L. W. Zhu, Y. B. Fu, G. B. Zhang, L. Sheng, and S. H. Yu, Cryst. Growth Des. **7**(8), 1423 (2007).
[28]Y. G. Su, G. S. Li, Y. F. Xue, and L. P. Li, J. Phys. Chem. C **111**(18), 6684 (2007).
[29]G. Blasse and L. H. Brixner, Chem. Phys. Lett. **173**(5–6), 409 (1990).
[30]D. Chen, G. Z. Shen, K. B. Tang, H. G. Zheng, and Y. T. Qian, Mater. Res. Bull. **38**(14), 1783 (2003).
[31]S. J. Chen, J. Li, X. T. Chen, J. M. Hong, Z. L. Xue, and X. Z. You, J. Cryst. Growth **253**(1–4), 361 (2003).
[32]Z. D. Lou and M. Cocivera, Mater. Res. Bull. **37**(9), 1573 (2002).
[33]L. G. Vanuitert and S. Preziosi, J. Appl. Phys. **33**(9), 2908 (1962).
[34]B. L. Chamberland, J. A. Kafalas, and J. B. Goodenough, Inorg. Chem. **16**(1), 44 (1977).
[35]T. Oi, K. Takagi, and T. Fukazawa, Appl. Phys. Lett. **36**(4), 278 (1980).
[36]J. P. Perdew and Y. Wang, Phys. Rev. B **45**(23), 13244 (1992).
[37]K. Tanaka, T. Miyajima, N. Shirai, Q. Zhuang, and R. Nakata, J. Appl. Phys. **77**(12), 6581 (1995).
[38]V. B. Mikhailik, H. Kraus, G. Miller, M. S. Mykhaylyk, and D. Wahl, J. Appl. Phys. **97**(8) (2005).
[39]P. Y. Jia, X. M. Liu, G. Z. Li, M. Yu, J. Fang, and J. Lin, Nanotechnology **17**(3), 734 (2006).
[40]Y. G. Wang, J. F. Ma, J. T. Tao, X. Y. Zhu, J. Zhou, Z. Q. Zhao, L. J. Xie, and H. Tian, Mater. Lett. **60**(2), 291 (2006).
[41]M. Maurera, A. G. Souza, L. E. B. Soledade, F. M. Pontes, E. Longo, E. R. Leite, and J. A. Varela, Mater. Lett. **58**(5), 727 (2004).
[42]A. Sen and P. Pramanik, J. Eur. Ceram. Soc. **21**(6), 745 (2001).
[43]W. S. Cho, M. Yashima, M. Kakihana, A. Kudo, T. Sakata, and M. Yoshimura, Appl. Phys. Lett. **66**(9), 1027 (1995).
[44]J. H. Ryu, J. W. Yoon, and K. B. Shim, Electrochem. Solid State Lett. **8**(5), D15 (2005).
[45]K. Tanaka, K. Fukui, K. Ohga, and C. K. Choo, J. Vac. Sci. Technol. A **20**(2), 486 (2002).
[46]P. F. Carcia, M. Reilly, C. C. Torardi, M. K. Crawford, C. R. Miao, and B. D. Jones, J. Mater. Res. **12**(5), 1385 (1997).
[47]Q. Y. Lu, F. Gao, and S. Komarneni, J. Mater. Res. **19**(6), 1649 (2004).
[48]V. Polshettiwar, M. N. Nadagouda, and R. S. Varma, Aust. J. Chem. **62**(1), 16 (2009).
[49]J. Perelaer, B. J. de Gans, and U. S. Schubert, Adv. Mater. **18**(16), 2101 (2006).
[50]N. L. Campbell, R. Clowes, L. K. Ritchie, and A. I. Cooper, Chem. Mater. **21**(2), 204 (2009).
[51]O. Yoshikawa, T. Sonobe, T. Sagawa, and S. Yoshikawa, Appl. Phys. Lett. **94**(8) (2009).
[52]V. Polshettiwar, M. N. Nadagouda, and R. S. Varma, Chem. Commun. (47), 6318 (2008).
[53]M. D. Roy, A. A. Herzing, S. Lacerda, and M. L. Becker, Chem. Commun. (18), 2106 (2008).
[54]H. Wang, F. D. Medina, D. D. Liu, and Y. D. Zhous, J. Phys.-Condens. Matter **6**(28), 5373 (1994).
[55]R. B. Pode and S. J. Dhoble, Phys. Status Solidi B **203**(2), 571 (1997).
[56]M. V. Nazarov, B. S. Tsukerblat, E. J. Popovici, and D. Y. Jeon, Phys. Lett. A **330**(3–4), 291 (2004).
[57]M. J. Treadaway and R. C. Powell, Phys. Rev. B **11**(2), 862 (1975).
[58]J. Geng, J. J. Zhu, D. J. Lu, and H. Y. Chen, Inorg. Chem. **45**(20), 8403 (2006).
[59]J. W. Yoon, J. H. Ryu, and K. B. Shim, Mater. Sci. Eng. B **127**(2–3), 154 (2006).
[60]P. Hohenberg and W. Kohn, Phys. Rev. B **136**(3B), B864 (1964).
[61]W. Kohn and L. J. Sham, Phys. Rev. **140**(4A), 1133 (1965).
[62]C. Cheng, K. Kunc, G. Kresse, and J. Hafner, Phys. Rev. B **66**(8), 085419 (2002).
[63]O. Levy, R. V. Chepulskii, G. L. W. Hart, and S. Curtarolo, J. Am. Chem. Soc. **132**(2), 833 (2010).
[64]A. R. Akbarzadeh, C. Wolverton, and V. Ozolins, Phys. Rev. B **79**(18), 184102 (2009).
[65]J. S. Hummelshoj, D. D. Landis, J. Voss, T. Jiang, A. Tekin, N. Bork, M. Dulak, J. J. Mortensen, L. Adamska, J. Andersin, J. D. Baran, G. D. Barmparis, F. Bell, A. L. Bezanilla, J. Bjork, M. E. Bjorketun, F. Bleken, F. Buchter, M. Burkle, P. D. Burton, B. B. Buus, A. Calborean, F. Calle-Vallejo, S. Casolo, B. Chandler, D. H. Chi, I. Czekaj, S. Datta, A. Datye, A. DeLaRiva, V. Despoja, S. Dobrin, M. Engelund, L. Ferrighi, P. Frondelius, Q. Fu, A. Fuentes, J. Furst, A. Garcia-Fuente, J. Gavnholt, R. Goeke, S. Gudmundsdottir, K. D. Hammond, H. Hansen, D. Hibbitts, E. Hobi, J. G. Howalt, S. L. Hruby, A. Huth, L. Isaeva, J. Jelic, I. J. T. Jensen, K. A. Kacprzak, A. Kelkkanen, D. Kelsey, D. S. Kesanakurthi, J. Kleis, P. J. Klupfel, I. Konstantinov, R. Korytar, P. Koskinen, C. Krishna, E. Kunkes, A. H. Larsen, J. M. G. Lastra, H. Lin, O. Lopez-Acevedo, M. Mantega, J. I. Martinez, I. N. Mesa, D. J. Mowbray, J. S. G. Myrdal, Y. Natanzon, A. Nistor, T. Olsen, H. Park, L. S. Pedroza, V. Petzold, C. Plaisance, J. A. Rasmussen, H. Ren, M. Rizzi, A. S. Ronco, C. Rostgaard, S. Saadi, L. A. Salguero, E. J. G. Santos, A. L. Schoenhalz, J. Shen, M. Smedemand, O. J. Stausholm-Moller, M. Stibius, M. Strange, H. B. Su, B. Temel, A. Toftelund, V. Tripkovic, M. Vanin, V. Viswanathan, A. Vojvodic, S. Wang, J. Wellendorff, K. S. Thygesen, J. Rossmeisl, T. Bligaard, K. W. Jacobsen, J. K. Norskov, and T. Vegge, J. Chem. Phys. **131**(1), 014101 (2009).
[66]S. P. Ong, L. Wang, B. Kang, and G. Ceder, Chem. Mater. **20**(5), 1798 (2008).
[67]J. Greeley, T. F. Jaramillo, J. Bonde, I. B. Chorkendorff, and J. K. Norskov, Nature Mater. **5**(11), 909 (2006).
[68]S. Curtarolo, D. Morgan and G. Ceder, CALPHAD: Comput. Coupling Phase Diagrams Thermochem. **29**(3), 163 (2005).
[69]A. B. Campos, A. Z. Simoes, E. Longo, J. A. Varela, V. M. Longo, A. T. de Figueiredo, F. S. De Vicente, and A. C. Hernandes, Appl. Phys. Lett. **91**(5), 051923 (2007).
[70]S. L. Porto, E. Longo, P. S. Pizani, T. M. Boschi, L. G. P. Simoes, S. J. G. Lima, J. M. Ferreira, L. E. B. Soledade, J. W. M. Espinoza, M. R. Cassia-Santos, M. Maurera, C. A. Paskocimas, I. M. G. Santos, and A. G. Souza, J. Solid State Chem. **181**(8), 1876 (2008).
[71]L. Gracia, J. Andrés, V. M. Longo, J. A. Varela, and E. Longo, Chem. Phys. Lett. **493**, 141 (2010).
[72]R. Dovesi, V. R. Saunders, C. Roetti, R. Orlando, C. M. Zicovich-Wilson, F. Pascale, B. Civalleri, K. Doll, N. M. Harrison, I. J. Bush, P. D'Arco, and M. Llunell, CRYSTAL06 User's Manual (University of Torino, 2006).
[73]A. D. Becke, J. Chem. Phys. **98**(7), 5648 (1993).
[74]C. T. Lee, W. T. Yang, and R. G. Parr, Phys. Rev. B **37**(2), 785 (1988).
[75]C.-H. Hu and D. P. Chong, *Encyclopedia of Computational Chemistry* (Wiley, Chichester, 1998).
[76]K. Momma and F. Izumi, J. Appl. Crystallogr. **41**, 653 (2008).
[77]B. Ravel and M. Newville, Phys. Scr., T **115**, 1007 (2005).
[78]B. Ravel and M. Newville, J. Synchrotron Radiat. **12**, 537 (2005).
[79]K. J. Rao, B. Vaidhyanathan, M. Ganguli, and P. A. Ramakrishnan, Chem. Mater. **11**(4), 882 (1999).
[80]G. J. Wilson, A. S. Matijasevich, D. R. G. Mitchell, J. C. Schulz, and G. D. Will, Langmuir **22**(5), 2016 (2006).
[81]A. T. de Figueiredo, V. M. Longo, S. de Lazaro, V. R. Mastelaro, F. S. De Vicente, A. C. Hernandes, M. S. Li, J. A. Varela, and E. Longo, J. Lumin. **126**(2), 403 (2007).
[82]P. N. Lisboa-Filho, V. R. Mastelaro, W. H. Schreiner, S. H. Messaddeq, M. S. Li, Y. Messaddeq, P. Hammer, S. J. L. Ribeiro, P. Parent, and C. Laffon, Solid State Ionics **176**(15–16), 1403 (2005).
[83]S. de Lazaro, J. Milanez, A. T. de Figueiredo, V. M. Longo, V. R. Mastelaro, F. S. De Vicente, A. C. Hernandes, J. A. Varela, and E. Longo, Appl. Phys. Lett. **90**(11), 111904 (2007).

[84]F. M. Pontes, C. D. Pinheiro, E. Longo, E. R. Leite, S. R. de Lazaro, R. Magnani, P. S. Pizani, T. M. Boschi, and F. Lanciotti, J. Lumin. **104**(3), 175 (2003).
[85]V. M. Longo, L. S. Cavalcante, R. Erlo, V. R. Mastelaro, A. T. de Figueiredo, J. R. Sambrano, S. de Lazaro, A. Z. Freitas, L. Gomes, N. D. Vieira, J. A. Varela, and E. Longo, Acta Material. **56**(10), 2191 (2008).
[86]Y. Kou, B. Zhang, J. Z. Niu, S. B. Li, H. L. Wang, T. Tanaka, and S. Yoshida, J. Catal. **173**(2), 399 (1998).
[87]A. Kuzmin and J. Purans, Radiat. Meas. **33**(5), 583 (2001).
[88]G. L. Poirier, F. C. Cassanjes, Y. Messaddeq, S. J. L. Ribeiro, A. Michalowicz, and M. Poulain, J. Non-Cryst. Solids **351**(46–48), 3644 (2005).
[89]S. Yamazoe, Y. Hitomi, T. Shishido, and T. Tanaka, J. Phys. Chem. C **112**(17), 6869 (2008).
[90]A. Kuzmin, J. Purans, and R. Kalendarev, Ferroelectrics **258**(1–4), 313 (2001).
[91]O. Y. Khyzhun, J. Alloys Compd. **305**(1–2), 1 (2000).
[92]O. Y. Khyzhun, V. L. Bekenev, and Y. M. Solonin, J. Alloys Compd. **480**(2), 184 (2009).
[93]J. Moscovici, A. Rougier, S. Laruelle, and A. Michalowicz, J. Chem. Phys. **125**(12), 124505 (2006).
[94]D. Errandonea, R. S. Kumar, L. Gracia, A. Beltran, S. N. Achary, and A. K. Tyagi, Phys. Rev. B **80**(9), 094101 (2009).
[95]L. Gracia, A. Beltran, and D. Errandonea, Phys. Rev. B **80**(9), 094105 (2009).
[96]S. Qin, X. Wu, F. Seifert, and A. I. Becerro, J. Chem. Soc. Dalton Trans. (19), 3751 (2002).
[97]A. N. Vtyurin, A. Bulou, A. S. Krylov, M. L. Afanas'ev, and A. P. Shebanin, Phys. Solid State **43**(12), 2307 (2001).
[98]R. M. Hazen, L. W. Finger, and J. W. E. Mariathasan, J. Phys. Chem. Solids **46**(2), 253 (1985).
[99]J. C. Sczancoski, L. S. Cavalcante, M. R. Joya, J. A. Varela, P. S. Pizani, and E. Longo, Chem. Eng. J. **140**(1–3), 632 (2008).
[100]T. T. Basiev, S. V. Vassiliev, V. A. Konjushkin, V. V. Osiko, A. I. Zagumennyi, Y. D. Zavartsev, S. A. Kutovoi, and I. A. Shcherbakov, Laser Phys. Lett. **1**(5), 237 (2004).
[101]Y. K. Voron'ko, A. A. Sobol, V. E. Shukshin, A. I. Zagumennyi, Y. D. Zavartsev, and S. A. Kutovoi, Phys. Solid State **51**(9),1886 (2009).
[102]J. H. Ryu, G. S. Park, K. M. Kim, C. S. Lim, J. W. Yoon, and K. B. Shim, Appl. Phys. A **88**(4), 731 (2007).
[103]D. L. Wood and J. Tauc, Phys. Rev. B **5**(8), 3144 (1972).
[104]E. Orhan, M. Anicete-Santos, M. Maurera, F. M. Pontes, A. G. Souza, J. Andres, A. Beltran, J. A. Varela, P. S. Pizani, C. A. Taft, and E. Longo, J. Solid State Chem. **178**(4), 1284 (2005).
[105]W. F. Zhang, Z. Yin, and M. S. Zhang, Appl. Phys. A **70**(1), 93 (2000).
[106]W. F. Zhang, Z. Yin, M. S. Zhang, Z. L. Du, and W. C. Chen, J. Phys., Conds. Matter **11**(29), 5655 (1999).
[107]D. P. Volanti, M. O. Orlandi, J. Andres, and E. Longo, Crystengcomm. **12**(6), 1696–1699 (2010).
[108]V. M. Longo, L. S. Cavalcante, E. C. Paris, J. C. Sczancoski, P. S. Pizani, M. S. Li, J. Andrés, E. Longo, and J. A. Varela, J. Phys. Chem. C 10.1021/jp1082328 (2011).
[109]G. Blasse and M. Wiegel, J. Alloys Compd. **224**(2), 342 (1995).
[110]M. V. Korzhik, V. B. Pavlenko, T. N. Timoschenko, V. A. Katchanov, A. V. Singovskii, A. N. Annenkov, V. A. Ligun, I. M. Solskii, and J. P. Peigneux, Phys. Status Solidi A **154**(2), 779 (1996).
[111]E. V. Sokolenko, V. M. Zhukovskii, E. S. Buyanova, and Y. A. Krasnobaev, Inorg. Mater. **34**(5), 499 (1998).
[112]B. M. Sinelnikov, E. V. Sokolenko, and V. Y. Zvekov, Inorg. Mater. **32**(9), 999 (1996).
[113]R. Zhai, H. Wang, H. Yan, and M. Yoshimura, J. Cryst. Growth **289**(2), 647 (2006).
[114]Z. L. Wang, G. Z. Li, Z. W. Quan, D. Y. Kong, X. M. Liu, M. Yu, and J. Lin, J. Nanosci. Nanotechnol. **7**(2), 602 (2007).
[115]X. Liu, P. Yu, Y. F. Tian, Y. Liu, and D. Q. Xiao, Ferroelectrics **383**, 27 (2009).
[116]T. Y. Liu, J. Chen, and F. N. Yan, J. Lumin. **129**(2), 101 (2009).
[117]V. M. Longo, A. T. de Figueiredo, A. B. Campos, J. W. M. Espinosa, A. C. Hernandes, C. A. Taft, J. R. Sambrano, J. A. Varela, and E. Longo, J. Phys. Chem. A **112**(38), 8920 (2008).
[118]C. Y. Pu, T. Y. Liu, and Q. R. Zhang, Phys. Status Solidi B **245**(8), 1586 (2008).
[119]M. L. Moreira, G. P. Mambrini, D. P. Volanti, E. R. Leite, M. O. Orlandi, P. S. Pizani, V. R. Mastelaro, C. O. Paiva-Santos, E. Longo, and J. A. Varela, Chem. Mater. **20**(16), 5381 (2008).
[120]P. Parhi, T. N. Karthik, and V. Manivannan, J. Alloys Compd. **465**(1–2), 380 (2008).
[121]V. M. Longo, L. S. Cavalcante, A. T. de Figueiredo, L. P. S. Santos, E. Longo, J. A. Varela, J. R. Sambrano, C. A. Paskocimas, F. S. De Vicente, and A. C. Hernandes, Appl. Phys. Lett. **90**(9), 091906 (2007).